An Introduction to Halo Nuclei

Jim Al-Khalili

Department of Physics, University of Surrey, Guildford, GU2 7XH, UK

Abstract. This lecture will not aim to provide an exhaustive review of the field of halo nuclei, but rather will outline some of the theoretical techniques that have been used and developed, both in structure and reaction studies, over the past decade to understand their properties. A number of review articles have recently appeared in the literature [1–10] which the interested reader can then go to armed with a basic understanding of how the theoretical results were produced.

1 What Is a Halo?

The field of halo nuclei has generated much excitement and many hundreds of papers since its discovery in the mid-1980s. While early β- and γ-decay studies of many of these nuclei yielded information about their lifetimes and certain features of their structure, credit for their discovery should go mostly to Tanihata [11,12] for the work of his group at Lawrence Berkeley Laboratory's Bevalac in 1985 on the measurement of the very large interaction cross sections of certain neutron-rich isotopes of helium and lithium, along with Hansen and Jonson for their pioneering paper two years later in which the term 'halo' was first applied to these nuclei [13]. Of course, it is worth mentioning that the first halo nucleus to be produced in the laboratory was ^{6}He, as long ago as 1936, using a beam of neutrons on a ^{9}Be target [14] just a few years after the discovery of the neutron! In contrast, the discovery of ^{11}Li, now regarded as the most famous halo nucleus, was not made until thirty years later [15], although its remarkable features had to wait a further two decades to be appreciated. We should begin therefore by defining just what constitutes a halo nucleus and under what conditions it will manifest itself.

The halo is a *threshold* effect arising from the very weak binding of the last one or two valence nucleons (usually neutrons) to, and hence decoupling from, a well-defined inert 'core' containing all the other nucleons. Textbook quantum mechanics states that the combination of weak binding and short range nuclear force (since the core is relatively compact) means that the neutron(s) can tunnel out into a volume well beyond the nuclear core and into the 'classically-forbidden' region. Consider for instance the eigenfunctions of a particle bound in a finite 1-D square well potential. Deeply-bound states are mostly confined within the potential and have very little extension beyond its walls. But states with eigen-energies just below the surface of the well will have slowly decaying exponential tails extending well beyond the range of

J. Al-Khalili, An Introduction to Halo Nuclei, Lect. Notes Phys. **651**, 77–112 (2004)
http://www.springerlink.com/

the potential. Quantum mechanically, this means that there is a significant probability of finding the particle outside of the well.

In halo nuclei, the potential well corresponds to the mean field potential of the rest of the nucleons in the nucleus. The valence nucleon (we will restrict the discussion to one halo nucleon for now) has a good chance of finding itself outside the core. The Uncertainty Principle ensures that such bound states have a relatively short lifetime, of the order of a few milliseconds to a few seconds. We will see that this is quite long enough for such nuclei to be formed and used in nuclear reactions in order to study their unusual features.

The accepted definition of a halo nucleus (typically in its ground state) is therefore that the halo neutron is required to have more than 50% of its probability density outside the range of the core potential. In such an open structure, it is not surprising that shell model and mean field approaches to describe such systems break down, and that few-body (cluster) models of core plus valence particles can account for the most general properties of these nuclei, such as their large size and breakup cross sections.

In addition to the decoupling of core and valence particles and their small separation energy, the other important criterion for a halo is that the valence particle must be in a low relative orbit angular momentum state, preferable an s-wave, relative to the core, since higher l-values give rise to a confining centrifugal barrier. The confining Coulomb barrier is the reason why proton halos are not so spatially extended as neutron halos.

Since halo nuclei are short-lived they must be studied using radioactive beam facilities is which they are formed and then used to initiate a nuclear reaction with a stable target. Indeed, most of what is know about halo nuclei comes from high energy fragmentation reactions in which the halo projectile is deliberately broken up and its fragments detected.

1.1 Examples of Halo Nuclei

The three most studied halo nuclei are ^{6}He, ^{11}Li and ^{11}Be. However, a few others have also now been confirmed, such as ^{14}Be, ^{14}B, ^{15}C and ^{19}C. All the above are examples of neutron halo systems, and all lie on, or are close to, the neutron dripline at the limits of particle stability. Other candidates, awaiting proper theoretical study and experimental confirmation include ^{15}B, ^{17}B and ^{19}B, along with ^{22}C and ^{23}O. Proton halo nuclei are not quite as impressive in terms of the extent of their halo, due to the confining Coulomb barrier which holds them closer to the core. Nevertheless, examples include ^{8}B, ^{13}N, ^{17}Ne and the first excited state of ^{17}F. We will deal for the most part here with the neutron halos. Another special feature is that most halos tend to be manifest in the ground states of the nuclei of interest. Indeed, most of the known halo nuclei tend to only have one bound state; any excitation of such a weakly bound system tends to be into the continuum, with the notable exception of ^{11}Be which has two bound states.

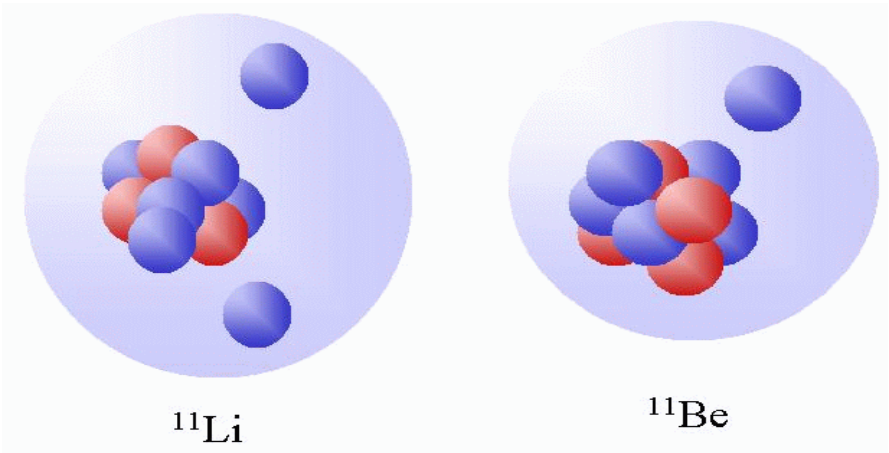

Fig. 1. The two most studied cases are the two-neutron halo nucleus ^{11}Li and the one-neutron halo nucleus ^{11}Be.

Excited state halos are less well studied. There is a danger of thinking that many nuclei will have excited states just below the one-neutron breakup threshold that exhibit halo-like features. After all, if the only criterion is that of weak binding then surely excited state halos would be everywhere. This is not the case, however, since, in addition, the core nucleons must be tightly bound together and spatially decoupled from the valence neutron.

1.2 Experimental Evidence for Halos

The first hint that something unusual was being seen came from the measurement of the electric dipole transition between the two bound states in ^{11}Be. Firstly, a simple shell model picture of the structure of ^{11}Be would suggest that its ground state should consist of a single valence neutron occupying the $0p_{1/2}$ orbital (the other six having filled the $0s_{1/2}$ and $0p_{3/2}$ orbitals). However, it was found that the $1s_{1/2}$ orbital drops down below the $0p_{1/2}$ and this 'intruder' state is the one occupied by the neutron, making it a $\frac{1}{2}^+$ ground state. The first excited state of ^{11}Be, and the only other particle bound state, is the $\frac{1}{2}^-$ state achieved when the valence neutron occupies the higher $0p_{1/2}$ orbital. The very short lifetime for the transition between these two bound states was measured in 1983 [16] and corresponded to an E1 strength of 0.36 W.u. It was found that this large strength could only be understood if realistic single particle wavefunctions were used to describe the valence neutron in the two states, which extended out to large distances due to the weak binding. Thus the radial integral involved in calculating the

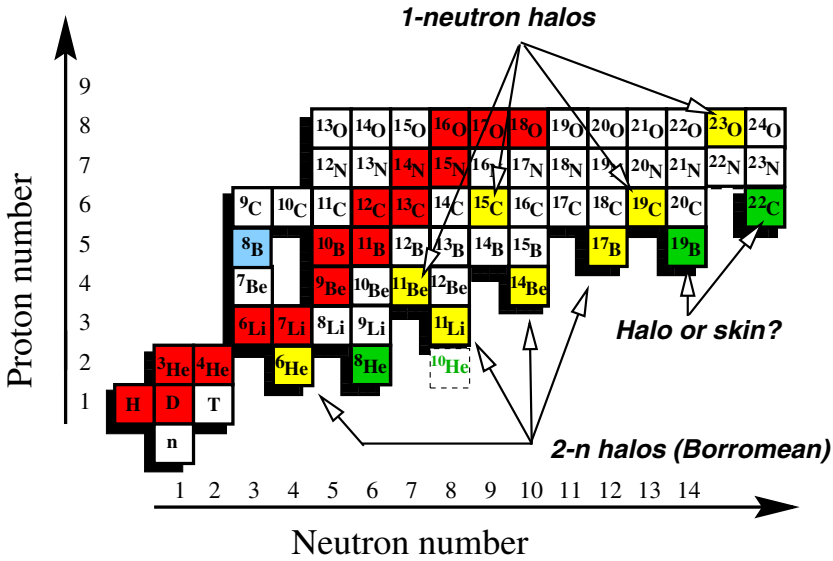

Fig. 2. A section of the Segre chart showing the halo nuclei.

transition had to be extended to a large distance, evidence of a long range tail to the wavefunction: the halo.

The Berkeley experiments carried out by Tanihata and his group in the mid-1980s involved the measurement of the interaction cross sections of helium and lithium isotopes and were found, for the cases of ^{6}He and ^{11}Li, to be much larger than expected. These corresponded to larger rms matter radii than would be predicted by the normal $A^{1/3}$ dependence. Hansen and Jonson [13] proposed that the large size of these nuclei is due to the halo effect. They explained the large matter radius of ^{11}Li by treating it as a binary system of ^{9}Li core plus a dineutron (a hypothetical point particle, implying the two neutrons are stuck together – of course the n-n system is unbound) and showed how the weak binding between this pair of clusters could form an extended halo density.

During the late eighties and early nineties, both theorists and experimentalists seemed satisfied with simple estimates of various halo properties by reproducing experimental reaction observables such as total reaction and Coulomb dissociation cross sections and momentum distributions following nuclear breakup. The high beam energies – the Berkeley experiments involved nuclear beams of about 800 MeV/nucleon – meant that semi-classical approaches could be reliably used in reaction models. More sophisticated numerical calculations, of both structure and reactions, have since been carried out over the past few years. Much of this article will be devoted to describing some of these models and showing how many of the formulae used to calculate certain observables are derived.

2 Structure Models

2.1 Two-Body Systems

Many of the general features of one-neutron halo nuclei can be studied using a simple 2-body (cluster) model of core + valence neutron bound by a short range potential. If the internal degrees of freedom of the nucleons in the core are decoupled from that of the single remaining valence neutron then we can simplify the many-body nuclear wavefunction,

$$\Phi_A \approx \phi_{\rm core}(\xi)\,\psi(\vec{r}) \ , \tag{1}$$

where ξ denotes the core's intrinsic coordinates and $\psi(\vec{r})$ is the bound state wavefunction of relative motion of core and valence neutron. One of the criteria for a halo state to exist is if the total probability for the neutrons to be found outside the range of the potential is greater than the corresponding probability within the potential (i.e. the neutron is most likely to be found beyond the reach of the potential that is binding it to the core). Outside the potential, the wavefunction has a simple Yukawa form

$$\psi(r) = N\frac{e^{-\kappa r}}{\kappa r} \ , \tag{2}$$

which describes its asymptotic behaviour and depends only on the binding (or 'separation') energy of the neutron via

$$\kappa = \frac{\sqrt{2\mu S_n}}{\hbar} \ , \tag{3}$$

where μ is the reduced mass of the core-neutron system and S_n is the separation energy. Clearly, the closer S_n is to zero, the slower the wavefunction falls to zero (see Fig. 3).

For halo nuclei, therefore, the dominant part of the wavefunction lies outside the potential and most of the physics comes from the behaviour of its tail. Indeed, its properties depend little on the shape of the potential. The mean square radius of such a wavefunction is thus

$$\langle r^2 \rangle = \frac{\int r^4\,dr\,(e^{-\kappa r}/\kappa r)^2}{\int r^2\,dr\,(e^{-\kappa r}/\kappa r)^2} = \frac{\hbar^2}{4\mu S_n} \ . \tag{4}$$

That is, the rms radius of the halo is inversely proportional to the square root of the separation energy. Such a diverging radius as the separation energy tends to zero is only true for orbital angular momenta $\ell = 0, 1$. This explains why halo states require low relative angular momentum for the valence particle, as well as weak binding. For $\ell \geq 2$ the radius converges with decreasing separation energy since the centrifugal barrier pushes the bound state into the potential. Necessary and sufficient conditions for the formation

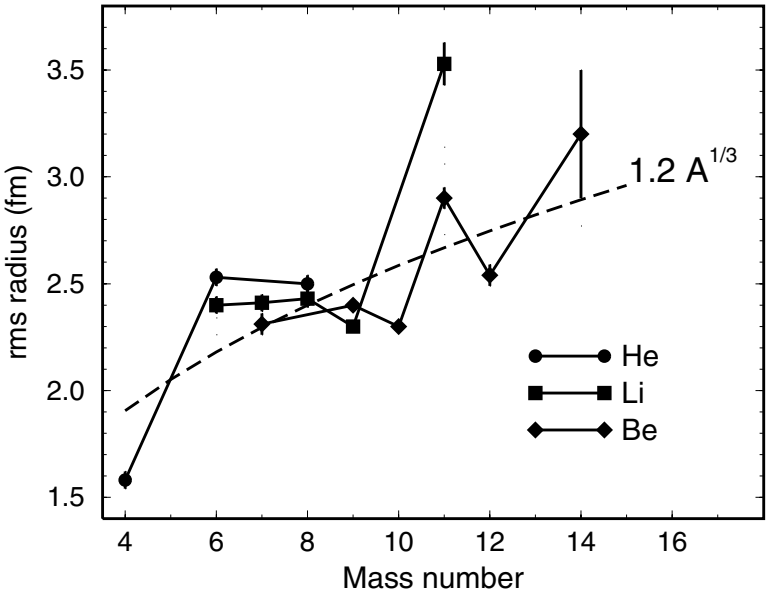

Fig. 3. A plot of the matter radii of isotopes of He, Li and Be as predicted by reaction cross section measurements and deduced from Glauber model calculations [17,18]

of a halo have been investigated [19] and universal scaling plots that relate radii to binding energies can be used to evaluate possible halo candidates [20].

Quite realistic wavefunctions for one-neutron halo nuclei such as ^{11}Be can be modelled by solving the 2-body bound state problem with a Woods-Saxon binding potential of appropriate geometry and with the depth chosen to produce the correct separation energy.

An obvious question is whether a halo is assumed to have formed whenever the last valence neutron is weakly bound (one MeV or less) and in a relative s or p state. Clearly, while examples of ground state nuclides with this feature are rare, there must be many examples of excited state just below threshold that have this feature. Many such states are unlikely, however, to represent clear halo signatures due to the high density of states in those regions. The core is unlikely to be tightly bound, inert and with internal degrees of freedom decoupled from the valence neutron. There are likely to be exceptions to this of course and one possible candidate is the 2^- state in ^{10}Be, which can be described roughly as an s-wave neutron bound by just 0.5 MeV to a ^{9}Be core. Whether the core is mainly in its ground state is questionable however.

Such simple models of one-neutron halo nuclei in terms of the neutron's single particle wavefunction are often not accurate enough to account for the physics that can now be accurately measured experimentally. Instead, one must go beyond this picture in which the core remains inert and in its

ground state. It is well accepted for instance that the loosely bound neutron in the $1/2^+$ ground state of ^{11}Be is mainly in an $s_{1/2}$ state, but there is also a significant core excited $^{10}\mathrm{Be}(2^+)$ component coupled to a $d_{5/2}$ neutron. Similar results are found in many other halo and exotic light nuclei.

We will deal in the next section with two-neutron halos, which have rather special features that deserve theoretical investigation. However, we end this section by considering briefly whether multineutron halos can exist. The difference in Fermi energies between neutrons and protons in nuclei leads to a more extended neutron density distribution than that of the protons. This difference is called the neutron skin and is a feature of most heavy nuclei. However, in such nuclei the neutron distribution has the same bulk and surface features (diffuseness) as the proton distribution. This is quite different to the halo, which is characterised by its long range and dilute nature. An example of a nucleus with features that are on the boundary between a halo and a skin is ^{8}He. This nucleus is well-described as an alpha core plus four valence neutrons. While it has a similar matter radius to its halo sister, ^{6}He, its valence neutron distribution does not extend out so far. It has therefore been remarked that, while ^{8}He is not a halo system, it is surrounded by such a thick neutron skin that it is akin to a mouse with the skin of an elephant. Clearly, the more valence neutrons there are outside the core, the more strongly their mutual attraction will hold them together, preventing a dramatic halo from forming.

2.2 Three-Body Systems – The Borromeans

Two-neutron halo nuclei, such as ^{6}He and ^{11}Li have the remarkable property that none of their two-body subsystems are bound. Thus, ^{6}He can be modelled as a bound three-body $\alpha + n + n$ system despite there being no bound states of $\alpha + n$ (^{5}He) or $n + n$ (the dineutron). Such nuclei have been dubbed 'Borromean' [21] and their wavefunctions require rather special asymptotic features to account for this behaviour.

The relative motion of the core and two neutrons is defined in terms of the Jacobi coordinates $(\vec{x}, \vec{y})$ as in Fig. 5. An extention of the one-neutron halo case suggests we can once again simplify the full many-body wavefunction by writing

$$\Phi_A \approx \phi_{\mathrm{core}}(\xi)\, \psi(\vec{x}, \vec{y}) \ , \tag{5}$$

where the relative wavefunction, ψ, is a solution of a three-body Schrödinger equation. While it is a non-trivial problem to calculate ψ, we can nevertheless reduce this 6-D equation to a one-dimensional 'radial' equation using hyperspherical coordinates $(\rho, \alpha, \theta_x, \varphi_x, \theta_y, \varphi_y)$ where $\rho = x^2 + y^2$ is the *hyperradius* and $\alpha = \tan^{-1}(x/y)$ is the hyperangle. Just as the 3-D equation describing the hydrogen atom (a 2-body system) is reduced to a radial one by separating out the angular dependence as spherical harmonics (eigenfunctions of

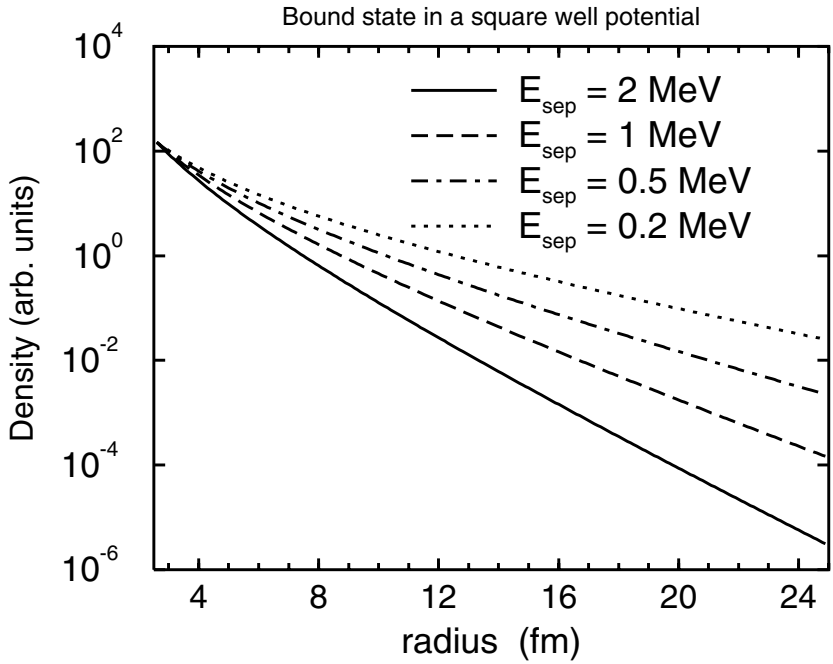

Fig. 4. The dependence of the wavefunction tail of a particle bound inside a square well potential on separation energy (the distance from the top of the well).

the angular momentum operator), we can again reach a 1-D equation in ρ by separating out all angular dependence within 'hyperspherical harmonics' [21]. Outside the range of the potential, the radial equation has the form

$$\left(-\frac{d^2}{d\rho^2} + \frac{(K+3/2)(K+5/2)}{\rho^2} - \frac{2mE}{\hbar^2}\right)\chi(\rho) = 0 \ , \tag{6}$$

where the new quantum number K is called the *hypermoment* and is the three-body extension of the orbital angular momentum quantum number. However, an important difference between this and the two-body case is that even for $K = 0$ (corresponding to relative s-waves between the two neutrons and between their centre of mass and the core) there is still a non-zero effective centrifugal barrier. The asymptotic behaviour of the 'radial' wavefunction is now of the form

$$\chi(\rho) \sim \frac{e^{-\kappa\rho}}{\rho^{5/2}} \ , \tag{7}$$

which is a generalisation of the Yukawa form (2) for the case of three-body asymptotics, where here $\kappa = \sqrt{2mS_{2n}}/\hbar$ involving the nucleon mass m and the two-neutron separation energy S_{2n}. Note here that we do not talk of the

separation energy for a single neutron since the Borromean nature of such systems means that if one of the halo neutrons is removed, the other will also 'fall off'.

The hyperradius, ρ, provides a useful measure of the extent of the halo for the case of Borromean nuclei since it depends on the magnitudes of both Jacobi coordinates. The overall matter radius of such systems is defined as

$$\langle r^2 \rangle = \frac{1}{A} \left((A-2) \langle r^2 \rangle_{\text{core}} + \langle \rho^2 \rangle \right) \ , \tag{8}$$

where $\langle r^2 \rangle_{\text{core}}$ is the intrinsic mean square radius of the core. A typical example with numbers is ^{11}Li: the radius of ^{9}Li is 2.3 fm while the root mean square hyperradius, describing the relative motion of the valence neutrons relative to the core, is about 9 fm. Together, these give a mass-weighted overall radius for ^{11}Li of about 3.5 fm.

It is of course questionable whether the above approach is a sensible way of defining the size of a halo nucleus. No one would suggest that the size of an atom be defined as the mass weighted sum of the sizes of its electron cloud and its nucleus. This is why many popular accounts of halo nuclei describe ^{11}Li as being the same size as a lead nucleus rather than, say, ^{48}Ca, which also has a radius of about 3.5 fm.

A number of elaborate techniques have been used to calculate the three-body wavefunctions of Borromean nuclei [21–26]. Such approaches assumed two-body pairwise potentials between the three constituents. It is important to treat the three-body asymptotic behaviour of the wavefunctions correctly in order to reproduce the basic features of these nuclei as well as the various reaction observables described in the next section.

2.3 Microscopic Models

Of course, projecting the full many-body wavefunction onto two- or three-body model spaces as was done in (1) and (5) is just an approximation. The few-body models of the structure of halo nuclei suffer from several shortcomings, namely that antisymmetrisation is often treated only approximately and that excitation and polarisation effects of the core are often ignored, although a number of studies are in progress to improve on these deficiencies. In favour of such cluster models of course is that the important few-body dynamics and asymptotics are included correctly. A number of studies are currently developing fully microscopic (*ab initio*) structure models. These are fully antisymmetric, start from a realistic NN interaction and can even include 3-body forces. The standard shell model fails to describe many of the essential features of halo nuclei (although it has proved to be of importance in providing spectroscopic information on a number of exotic nuclei) and many theorists acknowledge that there is a real need to go beyond the conventional shell model. For instance, the Continuum Shell Model and Gamow Shell Model [27] are showing promising early results. For very light systems,

progress is being made with the No-Core Shell Model [28], and the hope is that there will be a convergence of these two methods. But will they be able to predict a matter radius for ^{11}Li of 3.5 fm?

The acknowledged front runner among such *ab initio* microscopic structure models is the Greens Function Monte Carlo method (GMC) [29]. This approach involves calculating an approximate A-body wavefunction using the variational Monte Carlo method then using Greens function projection methods to obtain the desired bound state wavefunction. To date, the GMC method has been applied to describe the bound states of nuclei up to $A = 12$, including the halo states. However, it will have problems going to systems any higher in mass.

Another promising approach is the Coupled Cluster Method [30]. This has been used widely in a number of other fields such as chemistry and atomic and condensed matter physics and has only recently been applied seriously to nuclear structure. While still in its early stages, it has been tested successfully against GMC for ^{4}He. Its supporters are hopeful that it will be more successful in reaching heavier dripline nuclei than GMC.

No more will be said about such sophisticated methods here and the interested reader, as always, is directed to the listed references for further details.

3 Reaction Models

While there are many ways of probing the structure of nuclei through observing how they decay – and much has been learnt about halo nuclei from beta decay studies – I will focus here on nuclear reaction studies, which is the main activity in the field. It must be stressed that since halo nuclei are shortlived (less than a second) they cannot be used as a nuclear target. Instead they must form the beam that interacts with a stable target. Of course the physics is still the same and we can think of the reaction as taking place in 'inverse kinematics'.

During the late eighties and early nineties, both theorists and experimentalists seemed satisfied with quick and dirty estimates of various halo properties by reproducing experimental reaction observables, such as total reaction and Coulomb dissociation cross sections and momentum distributions following nuclear breakup. For instance, the rms matter radii were deduced by comparing calculated reaction cross sections with experimentally measured interactions cross sections [for such loosely-bound systems, these two quantities are essentially equal]. The high beam energies meant that semi-classical approaches, such as the Glauber model [31], could be reliably used. It will be shown later on how many useful formulae for reaction observables can be derived starting from the Glauber model, but it is worth pointing out that the basic expression for the total reaction cross section was around long before Glauber's work in the late 1950s and can be traced back to Hans Bethe in

1940. It relies on a simple geometric picture of the reaction process in which the target presents a circular disc blocking the path of the projectile. The reaction cross section is then an integral over impact parameter

$$\sigma_R = 2\pi \int_0^\infty b\, db\, (1 - T(b)) \tag{9}$$

where $T(b)$ is the probability of transmission (or the 'transparency'). It is this quantity that, in more sophisticated approaches, contains information about the density distributions of halo projectile and target nuclei. In fact, if one were to assume simple Gaussian density distributions for both nuclei, then an analytical expression can be evaluated for the reaction cross section [32]. The rms matter radius thus enters through the Gaussian parameter in the density. Such an analysis was used widely in the early work on halo nuclei and the deduced radii were known as 'experimental' ones on the assumption that the calculated reaction cross section was model independent. It has since been shown that this is not correct since the densities of halo nuclei are far from Gaussian shaped.

The momentum distribution of the fragments, following nuclear breakup of the halo projectile, was another observable analysed within a simple semi-classical (geometric) picture. By assuming that the target nucleus represented a fully absorptive black disk, then making a Serber (or sudden) approximation [33,34] (in which it is assumed that the surviving – non-absorbed – fragment continues with the same velocity as that of the incident beam) and neglecting any reaction mechanisms or final state interactions, it could be shown that the momentum distribution of the fragments was a good approximation to the momentum distribution of those clusters in the initial bound nucleus. The ground state wavefunction of the halo nucleus is thus just the Fourier Transform of the measured momentum distribution. Indeed the narrow distributions that were found for many of the halo candidates was confirmation of their large spatial extent.

It is indeed easy to show that, for a Yukawa wavefunction of the form of (2), its Fourier Transform gives a longitudinal momentum distribution of the (Breit-Wigner) form

$$\frac{d\sigma}{dp_\parallel} \propto \frac{1}{p^2 + \kappa^2}\ , \tag{10}$$

where κ was defined in (3). Clearly, the smaller the separation energy, and thus the smaller κ is, the narrower the momentum distribution. Figure 5 shows momentum distributions for a range of light nuclei. It is easy to spot those that have an extended spatial distribution due to a halo.

But of course, such simplistic models can only tell us basic information, and we need to work harder. In particular, in modelling reactions involving halo nuclei, it is important to note that the few-body correlations that are built into these structure models have to be retained. An important consideration in the study of reactions with halo nuclei is that they are easily

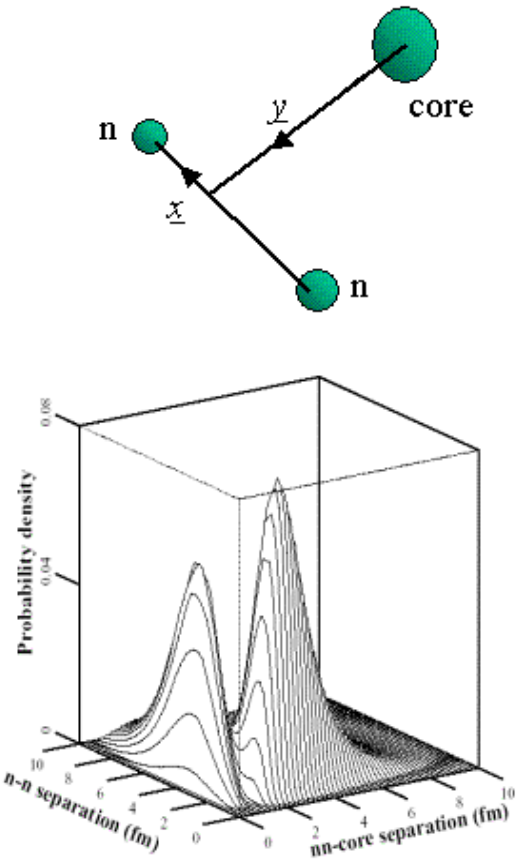

Fig. 5. Top: The Jacobi vectors of a three-body system. Bottom: A correlation density plot of the ground state of ^{6}He against the two Jacobi coordinates.

broken up in the nuclear and Coulomb fields of the target nucleus. Therefore, excitations of the halo nucleus into the continuum must be included in the reaction model. Such intermediate state coupling rules out 'one-step' models such as DWBA for many reactions of interest. It has been shown that any reliable reaction model must also take into account the few-body nature of these nuclei.

In parallel with advances in developing few-body structure models, therefore, theorists also developed few-body reaction models. At high (fragmentation) energies at which many of the experiments have been performed, a number of simplifying assumptions can be made to make the calculation of the reaction observables both tractable and transparent.

The most precise method of dealing with this problem is to map the continuum onto a discrete square-integrable basis that is orthogonal to the

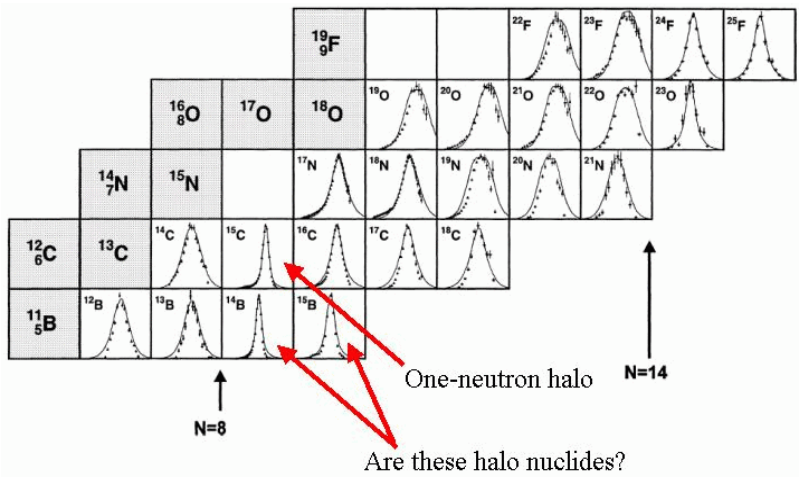

Fig. 6. The lngitudinal momentum distributions for the core fragments following single neutron removal from a range of neutron-rich nuclides on a carbon target [35]. The narrow the distribution, the larger the size of the nucleus.

bound states. This amounts to "chopping up" the continuum into energy bins that act as effective discrete excited states of the projectile and allows the problem to be solved within a (finite number of) coupled channels approach. This is the so called coupled discretised continuum channels (CDCC) method [36,37] that will be introduced in Sect. 4.6.

Another common approach is to make use of the adiabatic, or 'sudden', approximation [38] whereby it is assumed that the interaction time between the projectile and target is sufficiently short that the halo degrees of freedom can be regarded as frozen. This will be discussed in more depth in Sect. 3.7.

The most successful few-body approach for calculating probabilities and cross sections for a range of reactions involving halo nuclei has been based on Glauber's multiple scattering diffraction theory for composite systems [31, 39]. This model requires making an eikonal assumption in addition to the sudden approximation. This will be discussed in more detail next.

Few-body reactions at lower incident energies are far more difficult to treat consistently. Not only do nuclear and Coulomb interactions need to be treated within the same model to account correctly for interference effects, but multistep processes are even more important than at higher energies. An advantage of the CDCC method is its applicability at low energies where approximation schemes used in many other few-body approaches break down.

3.1 The Glauber Model

The theoretical study of scattering and reactions involving halo nuclei at the relatively high fragmentation beam energies at which so many of the

experiments have been conducted has led to a renaissance of a number of semi-classical reaction models. In particular, the Glauber model, which was first applied to nuclear scattering in the late 1950s, provides a remarkably simple framework for calculating various important observables arising from experiments involving loosely-bound projectiles such as halo nuclei. Its central assumption is the eikonal approximation: that the projectile travels along a definite straight line trajectory through the field of the target nucleus allows for the derivation of a number of crucial yet simple cross section formulae. It forms the basis for the reaction cross section expression that was used to analyse the early interaction cross section measurements which confirmed the large halo size. Later, a few-body generalisation of the Glauber model was used to provide a more accurate prediction for this size, and provided the first realistic calculation - one that included the important few-body structure information of the halo - of elastic scattering angular distributions for a number of nuclei such as ^{6}He, ^{8}He, ^{11}Be, ^{11}Li and ^{14}Be. Even today, it is such an important tool in reaction theory studies that it is worth discussing in some detail.

Let us first examine conditions for the validity of the eikonal approximation. Consider the scattering of a point particle from a potential with strength V_0 and range a. We can define a quantity τ_1 as the time spent by the projectile in the interaction region:

$$\tau_1 = \frac{a}{v} \ , \tag{11}$$

where $v = \hbar k/m$ is the classical velocity of the projectile. Also,

$$\tau_2 = \frac{\hbar}{|V_0|} \ , \tag{12}$$

is the time necessary for the scattering potential to have a significant effect on the projectile. The ratio of these two times, a 'coupling parameter', is thus

$$\frac{\tau_1}{\tau_2} = \frac{|V_0|a}{\hbar v} \ . \tag{13}$$

We therefore have two simple limits of this coupling parameter:

$$\begin{aligned} &1)\ \frac{\tau_1}{\tau_2} \ll 1 \Rightarrow \text{weak coupling limit (Born condition)} \\ &2)\ \frac{\tau_1}{\tau_2} \gg 1 \Rightarrow \text{strong coupling limit (WKB condition)} \ . \end{aligned} \tag{14}$$

In addition to these two limits, another way of distinguishing between the Born and WKB approximations is to think of the former as describing the scattering of waves (wavelike nature of projectile) whereas the latter describes particle scattering and is semi-classical in the sense of the projectile following a definite path or trajectory.

So what does the eikonal picture suggest? In common with other semi-classical approaches, the eikonal method is useful when the wavelength of the incident particle is short compared with the distance over which the potential varies appreciably. This short wavelength condition is expressed in terms of the incident wave number, k, and the range of the interaction, a, such that

$$ka \gg 1 \ . \tag{15}$$

However, unlike the short wavelength WKB approximation, the eikonal approximation also requires high scattering energies, such that

$$E \gg |V_0| \ . \tag{16}$$

It is helpful to re-express the coupling parameter of (13) in terms of these two conditions noting that we can write $\hbar v = \hbar^2 k/m = 2E/k$. Thus

$$\frac{\tau_1}{\tau_2} = \frac{|V_0|}{E} \times \frac{ka}{2} \ . \tag{17}$$

So while the eikonal approximation holds when the first factor is small and the second factor large, it says nothing about their product! In that sense, the eikonal approximation spans both the Born and WKB limits and contains elements of both. In practice, and when V is complex, the high energy condition is not critical and the eikonal approximation works well even when $E \approx |V_0|$ provided the first condition, (15), holds and we restrict ourselves to forward angle scattering. The reason for this is simple: a short range absorptive part to the scattering potential removes flux from the interior (small impact parameters) where the magnitude of the potential is large.

Since the potential varies slowly on the length scale of the incident wavelength, it is reasonable to extract the free incident plane wave from the scattering wave function as a factor, i.e.

$$\psi(\vec{R}) = e^{i\vec{k}\cdot\vec{R}}\,\omega(\vec{R}) \ , \tag{18}$$

where $\omega(\vec{R})$ is a modulating function and $\vec{R}$ is the projectile-target separation vector. The eikonal approximation can be derived starting from either the Schrödinger equation or the Lippmann-Schwinger equation. Here we follow the first approach. The scattering wave function of (18) is substituted in the Schrödinger equation

$$\left[\nabla_R^2 + k^2 - \frac{2\mu}{\hbar^2}V\right]\ e^{i\vec{k}\cdot\vec{R}}\ \omega(\vec{R}) = 0 \ , \tag{19}$$

where μ is the reduced mass. Using the eikonal conditions of (15) and (16) and with the coordinate z-axis along the incident wave vector $\vec{k}$, (19) reduces to the first order equation for ω

$$\frac{\partial\omega}{\partial z} = -\frac{i\mu}{\hbar^2 k}\,V\omega \ . \tag{20}$$

The solution of this equation, with the incident wave boundary condition requirement that $\omega(z \to -\infty) = 1$, is

$$\omega(\vec{R}) = \exp\left\{-\frac{i\mu}{\hbar^2 k}\int_{-\infty}^{z} V(x,y,z')dz'\right\}, \tag{21}$$

and yields the eikonal approximation to the wave function

$$\psi^{eik}(\vec{R}) = \exp\left\{i\vec{k}\cdot\vec{R} - \frac{i}{\hbar v}\int_{-\infty}^{z} V(x,y,z')dz'\right\}, \tag{22}$$

Thus, the modulating function introduces a modification to the phase of the incident plane wave that involves an integration along the direction of the incident beam and, as such, assumes that the effects of V are accurately accounted for by assuming the projectile traverses a straight line path. The eikonal method is therefore more accurate at forward scattering angles.

The scattering wavefunction of (22) has incorrect asymptotics since it does not look like incident plane wave plus outgoing spherical wave at $R \to \infty$. So, to calculate amplitudes and observables, it can only be used within a transition amplitude. For two-body elastic scattering via a central potential $V(R)$ the transition amplitude is

$$T(\vec{k},\vec{k'}) = \langle\vec{k'}|\ V\ |\psi_{\vec{k}}^{eik}\rangle\ . \tag{23}$$

This leads to the well-known form of the scattering amplitude

$$f(\theta) = -iK_0\int_0^{\infty} b\,db\,J_0(qb)\,[S_0(b)\ -\ 1]\ , \tag{24}$$

where $q = 2k\sin(\theta/2)$, θ is the cm scattering angle and $S_0(b) = \exp[i\chi(b)]$ is the eikonal elastic S-matrix element at impact parameter b. The eikonal phase shift function, $\chi(b)$, is defined as

$$\chi(b) = -\frac{1}{\hbar v}\int_{-\infty}^{\infty} V(R)\ dz\ . \tag{25}$$

In order to apply the Glauber model to reactions involving composite projectiles such as halo nuclei, we generalise the eikonal approach to what is called the Few-Body Glauber (FBG) model.

The FBG scattering amplitude, for a collision that takes a composite n-body projectile from an initial state $\phi_0^{(n)}$ to a final state $\phi_\alpha^{(n)}$, can be derived following the same steps as those in the two-body (point particle projectile) case. The post form transition amplitude is

$$T(\vec{K}_\alpha) = \langle\phi_\alpha^{(n)}\, e^{i\vec{K}_\alpha\cdot\vec{R}}|U(\{\vec{R}_j\})|\Psi_{\vec{K}_0}^{eik}\rangle, \tag{26}$$

where U is the sum of projectile constituent-target interactions

$$U(\vec{R}_1,\cdots,\vec{R}_n) = \sum_{j=1}^{n} V_{jT}(\vec{R}_j)\ , \tag{27}$$

and $\Psi^{eik}_{\vec{K}_0}$ is the eikonal approximation to the full $(n+1)$-body scattering wavefunction defined as the generalisation of the eikonal wavefunction of (18) to

$$\Psi^{eik}_{\vec{K}_0} = e^{i\vec{K}_0\cdot\vec{R}}\,\omega(\{\vec{r}_i\},\vec{R})\,\phi_0^{(n)}(\{\vec{r}_i\})\ . \tag{28}$$

By substituting for the eikonal wavefunction in the transition amplitude we obtain

$$f^{(n)}(\vec{K}_\alpha) = -\frac{iK_0}{2\pi}\int d\vec{b}\,e^{i\vec{q}\cdot\vec{b}}\,\langle\phi_\alpha^{(n)}|S^{(n)}(\vec{b}_1,\cdots,\vec{b}_n)-1|\phi_0^{(n)}\rangle, \tag{29}$$

where

$$S^{(n)} = \exp\left[i\sum_{j=1}^{n}\chi_j(b_j)\right] = \prod_{j=1}^{n} S_j(b_j). \tag{30}$$

Thus the total phase shift is the sum of the phase shifts for the scattering of each of the projectile's constituents. This property of phase shift additivity is a direct consequence of the linear dependence of eikonal phases on the interaction potentials V_{jt}.

Corrections to the straight line assumption of the eikonal approximation have been calculated and allow the FBG approach to be applied at considerably lower energies than expected (below 20 MeV/A). The most straightforward approach is to replace the eikonal S-matrices by the physical ones, obtained by solving the Schrödinger equation exactly for each cluster-target (2-body) subsystem, and then retaining the simplicity of the impact parameter framework of the model [40] by utilising the semi-classical limit $bk = \ell + 1/2$.

The model generalises in a natural way when Coulomb forces are included in the projectile constituent-target potentials, V_{jT}.

3.2 The Optical Limit of the Glauber Model

The Glauber model can be simplified considerably at high energies when the interaction between each projectile constituent and the target is purely absorptive. In this case, each constituent S-matrix, $S_j(b_j)$, is calculated within the optical limit of the Glauber model [41]. Here, the eikonal phase shifts are calculated assuming a '$t\rho\rho$' approximation to the optical potentials, V_{jT}, using one-body densities for each j constituent and the target and an effective nucleon-nucleon amplitude, f_{NN}. The optical limit S-matrices are thus written as

$$S_j^{OL}(b) = exp\left[i\int_{-\infty}^{\infty} dz\int\int d\vec{r}_1\,d\vec{r}_2\,\rho_j(r_1)\rho_T(r_2)f_{NN}(|\vec{R}+\vec{r}_1-\vec{r}_2|)\right]. \tag{31}$$

For an absorptive zero range NN amplitude and an isospin zero target we have

$$f_{NN}(\vec{r}) = (i\bar{\sigma}_{NN}/2)\delta(\vec{r}) \tag{32}$$

where $\bar{\sigma}_{NN}$ is the average of the free nn and np total cross sections at the energy of interest, which enter through the use of the optical theorem.

It is important to note that we have not thrown away here the few-body correlations in the projectile since at this stage it is only the constituents' scattering via their individual S_j's that have been treated in OL. The few-body S-matrix is still defined according to (30). However, if all few-body correlations are also neglected then $S^{(n)}$ is replaced by S^{OL}, defined as for the individual S_j^{OL} but with ρ_j replaced by the one-body density for the whole projectile. In this case it can easily be shown that the full projectile-target OL S-matrix is equivalent to neglecting breakup effects in (29), i.e.,

$$S^{OL}(b) = \exp\left[\langle\phi_0^{(n)}|i\sum_{j=1}^{n}\chi_j(b_j)|\phi_0^{(n)}\rangle\right]. \tag{33}$$

This is discussed in more detail in [39].

3.3 Cross Sections in Glauber Theory

The Glauber model provides a convenient framework for calculating integrated cross sections for a variety of processes involving peripheral collisions between composite projectiles and stable targets. In particular, stripping reactions have been studied using approaches developed by Serber [33]. Variants of such methods are still in use today due to the simple geometric properties of the reaction processes at high energies.

In the few-body Glauber model, the differential cross section for the scattering process defined by (29) is

$$\left(\frac{d\sigma}{d\Omega}\right)_\alpha = |f^{(n)}(\vec{K}_\alpha)|^2, \tag{34}$$

and the total cross section for populating the final state α is thus

$$\begin{aligned}\sigma_\alpha &= \int d\Omega\ |f^{(n)}(\vec{K}_\alpha)|^2 \\ &= \int d\vec{b}\ |\langle\phi_\alpha^{(n)}|S^{(n)}|\phi_0^{(n)}\rangle - \delta_{\alpha 0}|^2\ .\end{aligned} \tag{35}$$

It should again be noted however that such an expression is only valid at high beam energies and low excitation energies since energy conservation is not respected in this model. When $\alpha = 0$, the total elastic cross section is

$$\sigma_{el} = \int d\vec{b}\ |1 - \langle\phi_0^{(n)}|S^{(n)}|\phi_0^{(n)}\rangle|^2. \tag{36}$$

The total cross section is also obtained from the elastic scattering amplitude, employing the optical theorem, to give

$$\sigma_{tot} = 2 \int d\vec{b} \left[1 - \Re \, \langle \phi_0^{(n)} | S^{(n)} | \phi_0^{(n)} \rangle \right]. \tag{37}$$

Hence, the total reaction cross section, defined as the difference between the above two cross sections, is

$$\sigma_R = \int d\vec{b} \left[1 - |\langle \phi_0^{(n)} | S^{(n)} | \phi_0^{(n)} \rangle|^2 \right] \tag{38}$$

$$= \int d\vec{b} \left[1 - |S_{\rm proj}|^2 \right], \tag{39}$$

which can be compared with (9). Note that above, the projectile S-matrix is in the form

$$S^{FB}(b) = \langle \phi_0^{(n)} | S^{(n)} | \phi_0^{(n)} \rangle \tag{40}$$

and is referred to as the projectile's few-body (FB) S-matrix. In the optical limit (OL), however, $S_{\rm proj}$ could be replaced by the form in (33). As we shall soon see, the FB and OL S-matrices give different answers. The simplest distinction between the two is when each projectile constituent cluster S-matrix S_j is calculated in optical limit, as in (31). In that case the elastic S-matrix S^{FB} will contain effects due to breakup of the projectile, whereas S^{OL}, which contains the projectile wavefunction in the exponent, does not.

For a projectile of total angular momentum j, (38) is more correctly written as:

$$\sigma_R = \frac{1}{2j+1} \int d\vec{b} \sum_{m,m'} \left[1 - |\langle \phi_{0m'}^{(n)} | S^{(n)} | \phi_{0m}^{(n)} \rangle|^2 \right]. \tag{41}$$

For projectiles with just one bound state, any excitation due to interaction with the target will be into the continuum. For such nuclei, which include the deuteron and many of the neutron halo nuclei (such as ^{6}He and ^{11}Li), it is possible to describe elastic breakup channels in which the target and each cluster in the projectile remain in their ground states. For simplicity of notation, we assume a two-body projectile with continuum wave function $\phi_{\vec{k}}$, where $\vec{k}$ is the relative momentum between the two clusters and, from (30), $S^{(2)}(b_1, b_2) = S_1(b_1) S_2(b_2)$ is understood. Elastic breakup, also referred to as diffractive dissociation, has amplitudes

$$f(\vec{k}, \theta) = -iK_0 \int d\vec{b} \, e^{i\vec{q}\cdot\vec{b}} \, \langle \phi_{\vec{k}\sigma} | S^{(2)} | \phi_{0m} \rangle. \tag{42}$$

Making use of the completeness relation (when there is only one bound state)

$$\int d\vec{k} \; |\phi_{\vec{k}\sigma}\rangle\langle\phi_{\vec{k}\sigma}| = 1 - |\phi_{0m}\rangle\langle\phi_{0m}| \tag{43}$$

the total elastic breakup cross section is

$$\sigma_{bu} = \frac{1}{2j+1} \int d\vec{b} \sum_{m,m'} \left[\langle \phi_{0m} | \ |S_1|^2 |S_2|^2 | \phi_{0m} \rangle \delta_{m,m'} - |\langle \phi_{0m'} | S_1 S_2 | \phi_{0m} \rangle|^2 \right] \tag{44}$$

The difference between the reaction and elastic breakup cross section is the absorption cross section,

$$\sigma_{abs} = \frac{1}{2j+1} \int d\vec{b} \sum_{m} \left[1 - \langle \phi_{0m} | \ |S_1|^2 |S_2|^2 | \phi_{0m} \rangle \right] \ , \tag{45}$$

which represents the cross section for excitation of either the target or one or both of the projectile clusters.

The above formula can be understood by examining the physical meaning of the product $|S_1|^2|S_2|^2$. The square modulus of each cluster S-matrix element, represents the probability that it survives intact following interaction with the target at impact parameter $\vec{b}_j$. That is, at most, it is elastically scattered. At large $\vec{b}_j$ $|S_j|^2 \to 1$ since the jth constituent passes too far from the target. The quantity $1 - |S_j|^2$ is therefore the probability that cluster j interacts with the target and is absorbed from the system. Such a simple picture is useful when studying stripping reactions in which one or more of the projectile's clusters are removed by the target while the rest of the projectile survives. Thus, the cross section for stripping cluster 1 from the projectile, with cluster 2 surviving, is given by

$$\sigma_{str} = \frac{1}{2j+1} \int d\vec{b} \sum_{m} \langle \phi_{0m} | |S_2|^2 [1 - |S_1|^2] | \phi_{0m} \rangle. \tag{46}$$

This cross section is seen to vanish if the interaction V_{1T} of constituent 1 with the target is non-absorptive, and hence $|S_1| = 1$.

3.4 The Binary Cluster Model

One of the uses of the Glauber approach is that it enables us to consider, and solve easily, reaction calculations that give insights into the underlying structure of halo nuclei. We mention here, for pedagogical reasons, an analytical extension of this approach.

Consider a simple composite projectile consisting of A nucleons that can be modelled as a two-cluster system: an A_c-nucleon 'core' cluster and an A_v-nucleon 'valence' cluster ($A_c + A_v = A$). The intrinsic matter distributions of the two clusters are described by one-body Gaussian densities defined as

$$\rho_{c,v}(r) = a_{c,v} \, e^{-r^2/\alpha_{c,v}^2} \ , \qquad a_{c,v} = \frac{A_{c,v}}{(\sqrt{\pi}\alpha_{c,v})^3} \tag{47}$$

with normalisations such that $\int d\vec{r}\,\rho_{c,v}(r) = A_{c,v}$. We also assume that the relative motion wavefunction of the two clusters is a $0s$ oscillator state such that

$$|\phi_0(\vec{r})|^2 = \frac{1}{(\sqrt{\pi}\alpha_{\rm rel})^3} e^{-r^2/\alpha_{\rm rel}^2} \ . \tag{48}$$

We can then use such a model to construct simple formulae for the reaction cross section within both few-body (FB) and optical limit (OL) approaches (by using both forms of the projectile S-matrix defined in (40,33) in (39).

By convoluting the individual cluster densities with their motion about the projectile centre of mass, we obtain the overall one-body density of the projectile

$$\rho_p(r) = \hat{a}_c\, e^{-r^2/\hat{\alpha}_c^2} + \hat{a}_v\, e^{-r^2/\hat{\alpha}_v^2} \ , \qquad \hat{a}_{c,v} = \frac{A_{c,v}}{(\sqrt{\pi}\hat{\alpha}_{c,v})^3} \tag{49}$$

with Gaussian range parameters

$$\hat{\alpha}_{c,v} = \sqrt{\alpha_{c,v}^2 + \left(\frac{A_{c,v}}{A}\right)^2 \alpha_{\rm rel}^2} \ . \tag{50}$$

Since individual mean square radii of Gaussian densities have a simple analytical expression:

$$\langle r^2\rangle_i = \frac{3}{2}\alpha_i^2 \ , \qquad (i = c, v, {\rm rel}) \ , \tag{51}$$

we can write the overall projectile mean square radius as

$$\langle r^2\rangle_p = \frac{3}{2}\left[\frac{A_c}{A}\hat{\alpha}_c^2 + \frac{A_v}{A}\hat{\alpha}_v^2\right] \tag{52}$$

$$= \frac{A_c}{A}\langle r^2\rangle_c + \frac{A_v}{A}\langle r^2\rangle_v + \frac{A_c A_v}{A}\langle r^2\rangle_{\rm rel} \ . \tag{53}$$

What is important to note here is the following. Given any split in nucleons between the two clusters, a fixed choice of the two component ranges, $\hat{\alpha}_c$ and $\hat{\alpha}_v$ fixes the overall projectile density (49) and its radius (51). However, crucially, this does not fix the projectile's underlying structure since $\hat{\alpha}_c$ and $\hat{\alpha}_v$ each depend on two variables: the intrinsic cluster size (through α_v, α_v) and their separation (through $\alpha_{\rm rel}$). This gives rise to an important distinction between the OL and FB calculations of the reaction cross section and the deduced projectile radius. By choosing spatially extended clusters with small relative separation of their centres we can obtain the same overall projectile density as one containing small intrinsic clusters that are highly separated. Both these very different structures would give rise to the same overall OL cross section. However, their FB cross sections will be quite different (see Fig. 8).

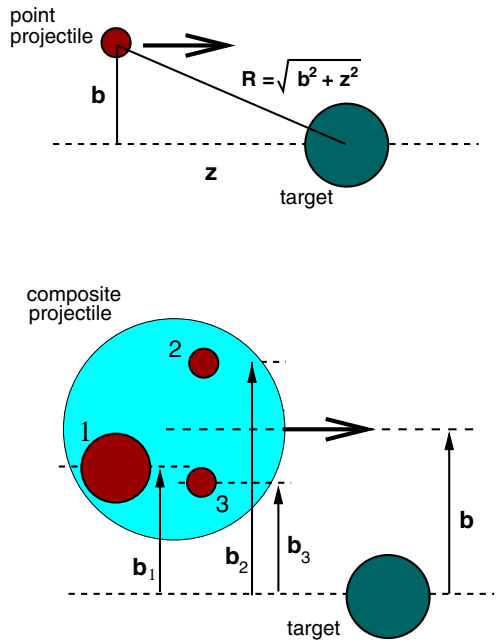

Fig. 7. Eikonal scattering. The straight line assumption of the eikonal approximation can be extended to incorporate a composite projectile, within the few-body Glauber model, where each constituent travels along a straight line path defined by its impact parameter with the target.

For the case of a one neutron halo nucleus, the situation is simpler. Now we set the valence cluster size to be pointlike ($\alpha_v = 0$ but will have a large relative separation between core and valence neutron. A given projectile density does now correspond to a unique underlying structure (for a given intrinsic core size) but, interestingly, we find that the OL and FB calculations still do not agree (Fig. 9). Indeed, Fig. 8 shows that for a constant overall projectile one-body density, a limiting case is when the valence cluster is pointlike and the cluster separation is a maximum (a halo). This gives rise to the maximum difference between the OL and FB calculations of the cross section.

The above general result is a consequence of the nature of the expressions for the two S-matrices in (33) and (40) and states that the OL cross section is always greater than the FB one. This result can be proved in the case of purely absorptive interactions between the clusters and the target and follows from the Johnson-Goebel inequality [42], which is described here due to its simplicity. Consider a real variable y. Due to the upward concavity of the exponential function we have

$$\exp(y) \geq 1 + y \ . \tag{54}$$

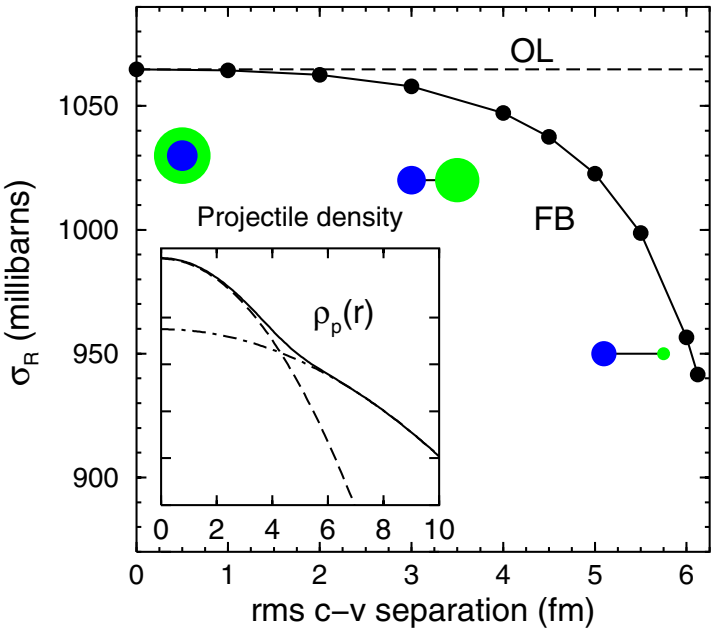

Fig. 8. The total reaction cross section for a projectile described by the two cluster model. The cross sections are calculated using two versions of the Glauber model: few-body (FB) and optical limit (OL). The projectile is assumed to have $A = 10$ with a mass spilt of $A_c = 8$, $A_v = 2$. The plot is against increasing cluster separation. However, since all calculations assume the same overall projectile one-body density, so increasing cluster separation must be balanced by a shrinking of the intrinsic cluster size. The OL calculation is not sensitive to this structure change whereas the FB one is.

This inequality is also valid if y is replaced by the expectation value of an Hermitian operator Y,

$$\langle \exp(Y) \rangle \geq \langle 1 + Y \rangle \ . \tag{55}$$

If we now replace Y by another Hermitian operator F such that $Y = F - \langle F \rangle$ then

$$\langle \exp(F) \rangle \geq \exp\langle F \rangle. \tag{56}$$

Therefore, by replacing F by $i \sum_{j=1}^{n} \chi_j(b_j)$ appearing in (30) and (33), which is real for absorptive V_{jt}, and taking its projectile ground state expectation value, we see that $S^{FB}(b) \geq S^{OL}(b)$ for all b. It follows therefore that $\sigma_R^{OL} \geq \sigma_R^{FB}$.

So we see that the explicit treatment of the few-body nature of the projectile in S^{FB} allows the inclusion of the effects of its breakup and results in a reduction of the calculated reaction cross section when compared to the

use of the no-breakup S^{OL}. Another way of stating this is that the collision is more transparent and less absorptive in the FB case. This is because, in many configurations of the spatially separated constituents, they do not overlap, and hence interact with, the target. This additional transparency due to the cluster nature of the projectile more than compensates for the additional absorption due to removal of flux from the elastic channel into the, now included, breakup channels.

It follows that if one compares measured high energy cross sections with those obtained from σ_R^{OL}, to deduce interaction radii, or nuclear sizes, then these sizes will be an underestimate of the actual spatial extent of the nuclei in those cases where the projectile has a well developed few-body internal structure (see Fig. 8).

3.5 More General Few-Body Reaction Models

We now take a step back from the Glauber model and ask whether the few-body problem can be solved without making any semi-classical assumptions. Clearly, solving the full $(A_P + A_T)$-body scattering problem exactly is not feasible. However, it can be reduced dramatically in complexity if we can ignore the target's internal structure and simplify the projectile from an A-body system to an n-cluster system as is done in the FBG model. Its ground state is assumed bound, with eigenfunction $\phi_0^{(n)}$. Each of its n constituents is assumed to interact with the target nucleus, T, via complex 2-body effective interactions V_{jT}. Thus, the target is allowed to be excited by each constituent separately. If the vector $\vec{R}$ joins the centre of masses of P and T then we must solve the $(n+1)$-body Schrödinger equation

$$\Big[T_R + U(\vec{R}_1, \cdots, \vec{R}_n) + H_P - E \Big] \Psi_{K_0}^{(+)}(\vec{r}_1, \cdots, \vec{r}_{n-1}, \vec{R}) = 0 \ , \qquad (57)$$

where T_R is the kinetic energy operator for the centre of mass of the projectile relative to the target, H_p is the projectile's internal Hamiltonian and U is the sum of projectile constituent-target interactions as defined in (27). Note that the $(n+1)$-body scattering wavefunction $\Psi_{K_0}^{(+)}$ is a function of $n-1$ independent vectors describing the projectile's internal motion along with the centre of mass vector $\vec{R}$. The n-body projectile intrinsic wavefunction satisfies

$$\begin{aligned} (H_P + \epsilon_0)\phi_0^{(n)} &= 0 \\ (H_P + \epsilon_k)\phi_{\vec{k}}^{(n)} &= 0 \ , \end{aligned} \qquad (58)$$

where $\phi_{\vec{k}}^{(n)}$ are eigenfunctions of excited states of the projectile. We assume here that there is only one bound state (the ground state) which is typical of most halo nuclei.

We must look for solutions of the full scattering equation of the form

$$\Psi^{(+)}_{K_0}(\{\vec{r}_i\},\vec{R}) = \phi^{(n)}_0(\{\vec{r}_i\})\chi_0(\vec{R}) + \int d\vec{k}\,\phi^{(n)}_{\vec{k}}(\{\vec{r}_i\})\chi_{\vec{k}}(\vec{R})\ . \tag{59}$$

The functions $\chi(\vec{R})$ give the amplitudes for exciting the projectile to unbound states. Note that the incident channel amplitude $\chi_0(\vec{R})$ also includes the incident plane wave.

By substituting for this wavefunction in the Schrödinger equation (57) we can follow standard procedures (see for instance textbooks by Satchler [44] and Feshbach [45]) to arrive at a set of coupled equations:

$$\Big[\, E_0 - T_R - Vii(\vec{R}) \,\Big]\, \chi_i(\vec{R}) = \sum_{j\neq i} V_{ij}(\vec{R})\,\chi_j(\vec{R})\ . \tag{60}$$

The coupling potentials are

$$V_{ij}(\vec{R}) = \int d\vec{r}_1\, d\vec{r}_2\, \cdots \phi^{(n)\,*}_i\, U\, \phi^{(n)}_j\ . \tag{61}$$

But this remains an impossible problem to solve exactly. Indeed, for halo nuclei, which are very weakly-bound and therefore easily broken up, coupling to the continuum is vital. This means there are an infinite number of coupled channels! Clearly approximation methods are required. We mention two of these models briefly here.

3.6 The CDCC Method

Even with the restricted model space of the $(n+1)$-body problem, the calculation of the full few-body scattering wavefunction $\Psi^{(+)}$ that can be used to obtain various scattering and reaction observables is not feasible. We therefore need theoretical schemes to approximate $\Psi^{(+)}$ while retaining the essential physics (such as the few-body dynamics and correlations).

The most accurate method available for the case of a two-cluster projectile (a 3-body problem) is that of the Coupled Discretised Continuum Channels (CDCC). In this method, the continuum is discretised into a finite number of energy bins, reducing the scattering problem to one involving a finite number of coupled channels. The method has been applied extensively to light nuclei that can be treated as two-cluster systems such as the deuteron $(p+n)$, ^{6}Li $(\alpha+d)$, ^{7}Li $(\alpha+t)$, ^{8}B (^{7}Be+p) and ^{11}Be (^{10}Be+n). The method cannot, however, be extended readily to three-body projectiles, such as the Borromean nuclei (^{6}He and ^{11}Li), although such a four-body CDCC model is under development.

The CDCC method approximates the three-body Schrödinger equation as a set of effective two-body coupled-channel equations by constructing a square integrable basis set $\{\phi_\alpha\}$ of relative motion states between the two

constituents of the projectile. Projectiles treated using the CDCC method tend to have very few bound states and the method provides a means of describing excitations to the continuum.

First, the continuum is truncated at a certain maximum, $k_{\max}$ and divided up into bins of width $\Delta k_i = k_i - k_{i-1}$, each of which is then regarded as a discrete excited state and represented by a normalised square integrable wavefunction describing the relative motion of the two clusters in the projectile. These bin states, together with the ground state, constitute an $(n+1)$ state coupled-channels problem for solution of the CDCC approximation to $\Psi^{(+)}$. Thus, (59) is replaced by the simpler

$$\Psi^{CDCC}(\vec{r},\vec{R}) = \sum_{i=0}^{N} \phi_i(\vec{r})\chi_i(\vec{R}), \tag{62}$$

where $i = 0$ refers to the projectile ground state.

Solution of the coupled equations leads to the calculation of the elastic or inelastic scattering amplitude required for observables such as the differential cross section angular distribution. Nuclear and Coulomb breakup of two-body projectiles can also be calculated with this model.

Convergence of the calculations have to be tested for different sizes of the model space. The number of bins and their upper limit depend on the particular state they are describing and the various parameters must be carefully chosen to describe the projectile continuum. Different schemes for construction of the bin states, as well as a more detailed discussion of the formalism, can be found in the literature [39].

3.7 The Adiabatic Model

This approach is a considerable simplification on the CDCC method provided the incident projectile energy is not too low. It assumes an 'adiabatic' (slowly varying) treatment of the projectile's internal motion while its centre of mass motion relative to the target is fast (a high energy approximation). Also referred to as the sudden approximation, it assumes the projectile's intrinsic degrees of freedom are frozen during the time taken for it to traverse the interaction region.

The most natural way of understanding how this approximation comes about is by considering the time-dependent Shrödinger equation (for a two-body projectile for simplicity):

$$H\Psi(\vec{R},\vec{r},t) = i\hbar\frac{\partial\Psi(\vec{R},\vec{r},t)}{\partial t} \ . \tag{63}$$

We then make the transformation

$$\Psi = e^{-i(H_P-\epsilon_0)t/\hbar}\Phi \ , \tag{64}$$

where H_P and ϵ_0 were defined earlier. Then, making the substitution into the Schrödinger equation

$$\left[T_R + \tilde{V}_1(\vec{R},\vec{r}(t)) + \tilde{V}_2(\vec{R},\vec{r}(t)) + \epsilon_0\right] \Phi = i\hbar \frac{\partial \Phi}{\partial t} \ , \tag{65}$$

where

$$\tilde{V}_j(\vec{R},\vec{r}(t)) = e^{i(H_P-\epsilon_0)t/\hbar}\ V_{jT}(\vec{R},\vec{r})\ e^{-i(H_P-\epsilon_0)t/\hbar} \qquad (j=1,2)\ . \tag{66}$$

In this so called 'Heisenberg picture' we have removed the projectile Hamiltonian H_P from the full H at the expense of placing the time-dependence in the potentials. And since H_P does not depend on $\vec{R}$ then we have

$$\tilde{V}_j(\vec{R},\vec{r}(t)) = V_{jT}(\vec{R},\vec{r(t)}) \ , \qquad \vec{r}(t) = e^{i(H_P-\epsilon_0)t/\hbar}\ \vec{r}\ e^{-i(H_P-\epsilon_0)t/\hbar}\ . \tag{67}$$

Hence, if $\vec{r}$ varies slowly with time then we can replace $\vec{r}(t)$ by $\vec{r}(0) = \vec{r}$. This is accurate provided the time spent by the projectile in the presence of the interactions is small (i.e $H_P - \epsilon_0)t/\hbar \ll 1$). We see now that we have reach a time-independent Schrödinger equation

$$\left[T_R + U(\vec{R},\vec{r}) - E + \epsilon_0\right] \Phi(\vec{R},\vec{r}) = 0 \tag{68}$$

in which the dependence on the projectile's internal coordinate $\vec{r}$ enters only as a parameter in the potentials and we have reduced the 3-body problem to a set of 2-body problems (one for each value of $\vec{r}$).

What is not so obvious at first sight is how we have dealt with the continuum of the projectile that is so important in halo scattering. Note that we have replaced H_P in the Schrödinger equation by the ground state binding energy ϵ_0. So now all eigenstates of the projectile are degenerate with the ground state. This assumption is good provided (1) $E \gg \epsilon_0$ and (2) the important continuum energies that the projectile is most likely to break up to also involve $\epsilon_k \ll E$.

The adiabatic approximation (often referred to in the context of halo scattering as the 'frozen halo' approximation) to the scattering wavefunction can be used, as in the case of the CDCC approach, to calculate various transition amplitudes for reactions of interest. Further details on this method can be found elsewhere [39].

It has been found recently that, contrary to what one might expect, the frozen halo approximation is valid even at incident energies as low as 10 MeV/nucleon or below [46]. This is because first order ('non-adiabatic') corrections mainly affect the scattering close to the target, where absorption effects dominate. Thus, provided the projectile core-target optical potential has a strong imaginary part, this approach is valid to quite low scattering energies.

Clearly, for two-body projectiles, the full CDCC approach is more accurate than the adiabatic approach, particularly at low energies. However, the

adiabatic model does not suffer so much from convergence issues or computational limitations. What is interesting from the point of view of the scattering of halo nuclei is that the adiabatic approximation allows for certain simplifying insights, such as when only one of the projectile's constituents interact with the target [47] (known as the recoil limit approximation and discussed in the next section) or when the zero range approximation is made in the case when the scattering wave function is required only at the point $\Psi^{AD}(\vec{R}, \vec{r} = 0)$ [48].

3.8 The Recoil Limit Approximation

Consider a one-neutron halo nucleus, such as ^{11}Be scattering elastically from a target. As described already, such a system can be treated within a three-body model of core + neutron + target. Assuming, in addition to the adiabatic approximation, that the valence neutron-target interaction is much weaker than the core-target interaction, we can set $V_n = 0$. In this case only the core feels the presence of the target. It can be shown [47,39] that in this situation the scattering amplitude factorises as

$$T(\vec{K}, \vec{K'}) = F(\vec{Q})\, \langle \vec{K'} | V_c(\vec{R}_c) | \chi^{(+)}_{\vec{K}} \rangle = F(\vec{Q})\, T_{pt}(\vec{K}, \vec{K'}), \tag{69}$$

where $\chi^{(+)}_{\vec{K}}(\vec{R}_c)$ is the two-body scattering wavefunction distorted by V_c, describing the scattering of the projectile, assumed pointlike, from this potential. Crucially, however, the important effects of the break-up of the halo projectile on the elastic scattering are retained in the form factor $F(\vec{Q})$ defined as

$$F(\vec{Q}) = \int d\vec{r} |\phi^{(2)}_0(\vec{r})|^2\, e^{i\vec{Q}\cdot\vec{r}}, \tag{70}$$

where $\vec{Q} = (\vec{K} - \vec{K'})/A$ is the momentum transfer to the valence particle during the scattering process.

This provides us with a useful formula for the cross section, which retains the important coupling between the weakly-bound halo g.s. wavefunction and the continuum of breakup channels, while providing a simple expression for the scattering cross section reminiscent of the expression for Born approximation scattering (although there is no Born approximation being made here):

$$\left(\frac{d\sigma}{d\Omega}\right)_{el} = |F(\vec{Q})|^2 \times \left(\frac{d\sigma}{d\Omega}\right)_{pt}. \tag{71}$$

The above formula shows how the scattering of an extended halo nucleus deviates (through the form factor) from the scattering of a point particle from the same potential. Figure 10 shows the application of this model to the elastic scattering of ^{11}Be. The recoil limit approximation clearly does

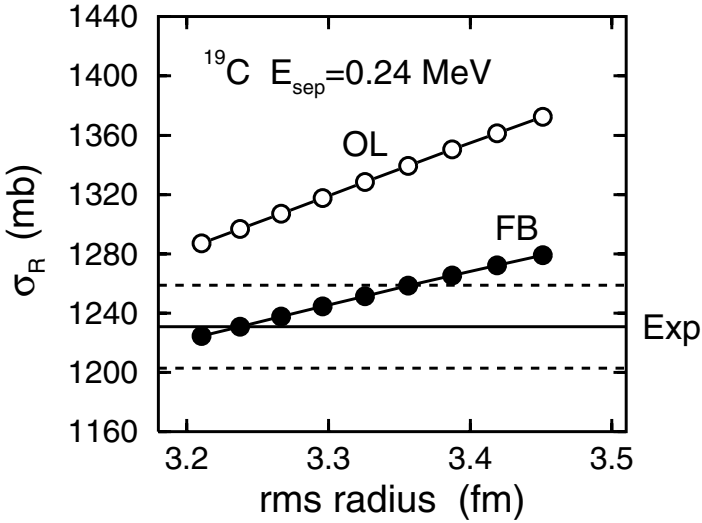

Fig. 9. The calculated reaction cross sections in the few-body model (solid symbols) and the optical limit approximation (open symbols), for ^{19}C+^{12}C at 960 MeV/nucleon, as a function of the rms radius of the ^{19}C. The halo neutron separation energy is taken to be 0.24 MeV and the two-body wavefunction for the projectile is calculated with a WS potential between the ^{18}C core and the valence neutron by searching on the potential depth to give the separation energy. The potential radius is kept fixed at $r_0 = 1.22$ fm while the diffuseness a was varied to obtain states with different rms radii. The horizontal lines represent the measured interaction cross section with its error bars. Further details can be found in [43]. The predicted radius is the one required for the theoretical calculation of the reaction cross section to fall within the error bars of the experimental cross section

very well in this case due to the large mass ratio of halo neutron and core (1/10). The long dashed curve is the point cross section due to scattering of ^{11}Be via the ^{10}Be potential only. The solid curve is the product this cross section and the square modulus of the form factor. The difference is due to the effects of breakup. This is highlighted by the folding model cross section (the no breakup limit) which is very close to the point cross section despite the inclusion of the valence potential.

3.9 Other Models

A number of other few-body reaction models have been developed and applied to reactions in which the projectile is treated as a core+valence nucleon system. These clearly deserve more than the brief mention afforded them in this lecture, but as always, the selection of topics reflects the author's prejudices. One method is to solve the time-dependent Schrödinger equation after assuming that the relative motion between the projectile's core and the tar-

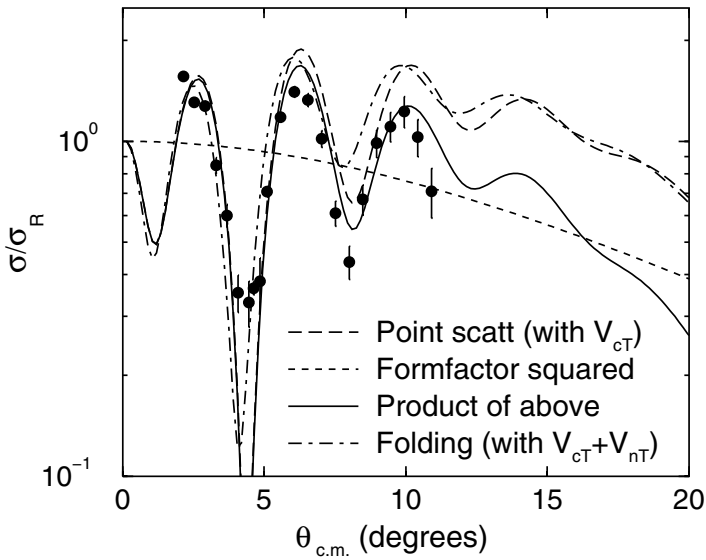

Fig. 10. Calculated differential cross sections for the elastic scattering of ^{11}Be from ^{12}C at about 50 MeV/nucleon showing the validity of the core recoil limit approximation. The curves are discussed in the text.

get can be treated classically and approximated by a constant velocity path. This method [49,50] treats the time dependence of the reaction explicitly and thus conserves energy, but not momentum. Breakup amplitudes can then be calculated within time dependent perturbation theory [51]. Other time dependent approaches [52,53] also treat the projectile-target relative motion semi-classically but solve the time dependent Schrödinger equation using a non-perturbative algorithm on a three-dimensional spatial mesh that allows the treatment of Coulomb breakup in the nonperturbative regime.

A very recent approach involves a combination of coupled channels approach such as CDCC and single-step Born Approximation to describe a particular reaction process such as a transfer reaction involving halo nucleons [54].

4 Results from Reaction Studies

4.1 Reaction Cross Sections

Early estimates of the size of neutron rich isotopes of lithium and helium employed the optical limit of the Glauber model [41] in which the nuclear one-body densities were taken to be simple Gaussians. They predicted an enhanced size for these nuclei compared with that obtained from the usual $\langle r^2 \rangle^{1/2} \propto A^{1/3}$ scaling. But by retaining the few-body degrees of freedom in the projectile wave function, its important structure information is retained,

as described in 3.4. As a consequence, studies that evaluated the reaction cross section within a few-body approach [17,18], rather than take the optical model limit, predicted an even larger matter radius, as shown in Fig. 9. This may at first sight seem contrary to what we might expect, since such a model allows for new breakup channels to become available, predicting a larger reaction cross section (and hence a smaller radius to bring the cross section back down to the experimental value again). However, the Johnson-Goebel inequality relation [42], discussed earlier, shows that for a given halo wave function, the optical limit model always *overestimates* the total reaction cross section for strongly absorbed particles, thus requiring a smaller halo size than suggested by the full few-body calculation.

4.2 Elastic and Inelastic Scattering

Much can been learned about the structure of nuclei from elastic scattering. But for unstable systems such as halo nuclei the scattering has to be carried out in inverse kinematics with the nucleus of interest as the beam scattering from a stable nucleus or single proton. Over the past decade, a number of measurements of the angular distribution for the scattering of halo nuclei from a stable target (often ^{12}C) were unable to distinguish between elastic and inelastic scattering due to the poor energy resolution in the detectors. Such 'quasielastic' cross sections were thus unable to resolve low-lying excited states of the target from the elastic channel and the data were an incoherent sum of elastic and inelastic pieces.

Angular distributions have been measured for the scattering of ^{6}He [55], ^{8}He [56], ^{8}B [57], ^{11}Li [58,59] and ^{14}Be [60]. Since most of these nuclei have only one bound state then any excitation they undergo during the scattering process will therefore couple to the breakup channels and the scattering will be strongly influenced by their dynamic polarization. For such projectiles, simple folding models based on single particle densities fail to generate the optical potentials needed to describe the elastic scattering angular distributions.

A more microscopic approach to elastic scattering is to use a few-body scattering model (based on a CDCC, adiabatic or Glauber approaches) in which the few-body correlations of the projectile are retained and breakup effects are included. Here it is the few-body wavefunction of the projectile that is used directly rather than its one-body density as well the projectile constituent-target optical potentials. One of the advantages of the Glauber approach is that breakup is included in a natural way to all continuum energies and angular momenta, and to all orders in breakup, through a closure relation. In fact, it has been found that higher order breakup terms, such as those responsible for continuum-continuum coupling, are indeed very important [61]. This topic is dealt with more carefully and in greater depth in the lecture by Alamanos and Gillibert in this volume.

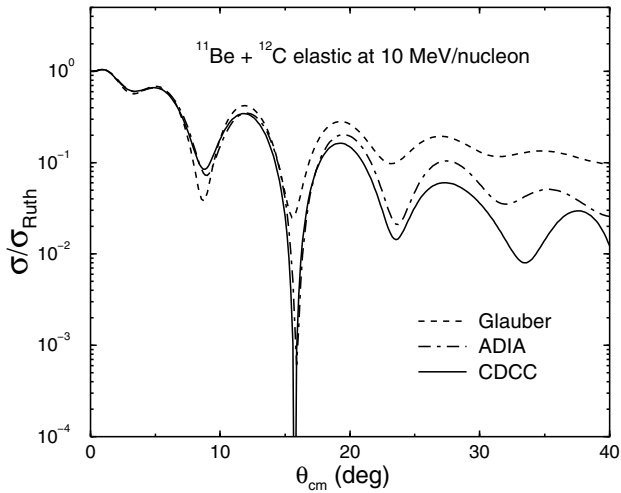

Fig. 11. Calculated differential cross sections for the elastic scattering of ^{11}Be from ^{12}C at 10 MeV/nucleon using various three-body models: Glauber (dashed curve), adiabatic (dot-dashed curve) and CDCC (solid curve) [40,46]. The importance of both non-adiabatic and non-eikonal corrections at larger scattering angles can be seen clearly at these relatively low scattering energies. No data exist at this energy.

4.3 Breakup Reactions

Halo nuclei are very weakly-bound and consequently easy to break up. It is therefore not surprising that breakup cross sections are much easier to measure than elastic ones. Numerous breakup measurements have been performed, even when the radioactive beam intensity was rather low. In parallel, the theoretical community has been attempting to model these reactions accurately.

The semiclassical theory for Coulomb excitation was developed in the early days of nuclear physics [62]. The approach is valid for large impact parameters and relies on the fact that the relative motion between the projectile and target can be treated classically whilst the excitation of the projectile is treated quantum mechanically. In this case, the total breakup cross section is a product of the Rutherford cross section by the square of the excitation amplitude. But while such a first order semiclassical method is appealing due to its simplicity, there are many aspects of the problem that are left out. One of the debated issues concerned the post-acceleration of the light fragment in the Coulomb field. In order to describe this process properly, one should formulate the problem non-perturbatively.

4.4 Momentum Distributions

Measurement of the momentum distributions of the fragments (core and valence nucleons) following the breakup of halo nuclei on stable targets is now

a well-established method for studying halo properties. While it has been used for many decades as a tool to access the structure of stable nuclei, it is particularly well-suited to loosely bound systems. The basic physics (described briefly in Sect. 3) is simple: since very little momentum transfer is required in the breakup process to dissociate the projectile fragments, they will be detected with almost the same velocity as they had prior to breakup, and their relative velocities will be very similar to those within the initial bound projectile. In all reactions with weakly-bound systems the momentum distributions are found to be very narrowly focussed about the beam velocity. Many measurements have been made, involving detection of both the valence nucleons and the core fragments, and the halo structure of several light nuclei has been established.

Two types of distributions can be measured: either perpendicular (transverse) or parallel (longitudinal) to the beam direction. Transverse distributions are more difficult to deal with theoretically since they are broadened due to nuclear and Coulomb diffraction effects (elastic scattering of the fragments from the target). This is why longitudinal momentum distributions are more widely used. Early on, simple models, based on eikonal assumptions agreed with measurements rather well. Similar widths were obtained from nuclear breakup on light targets and Coulomb breakup on heavy targets, supporting the view that the distributions were no more than the square of the Fourier Transform of the projectile ground state wavefunction. However, this view is considered too simplistic.

For single valence nucleon systems, the longitudinal inelastic breakup momentum distributions for the core - at high energies the elastic breakup piece is small - can be expressed within the Glauber framework as

$$\frac{\mathrm{d}\sigma}{\mathrm{d}k_z} = \frac{1}{2l+1} \sum_{m=-l}^{l} \int d\vec{s} \; \left| \frac{1}{\sqrt{2\pi}} \int dz \, e^{ik_z z} \, \phi_{lm}(\vec{s}, z) \right|^2 \times \int d\vec{b}_c \; |S_c(b_c)|^2 \left(1 - |S_n(b_n)|^2\right), \qquad (72)$$

where $b_n = |\vec{b}_c + \vec{s}|$ and $\vec{s}$ is the projection of the core-nucleon relative coordinate onto the impact parameter plane, $\phi_{lm}(\vec{s}, z)$ is the valence nucleon wavefunction with orbital angular momentum l and projection m, and S_c, S_n are the core and nucleon elastic S-matrices as described in Sect. 3.3. The integral over $\vec{b}$ in (72) represents the reaction mechanism and involves the product of the core survival probability (in its ground state) and the nucleon absorption probability by the target. Without this factor, the momentum distribution is just a Fourier transform of the nucleon wavefunction.

Reactions in which the halo neutron is knocked out of the projectile (known as knockout reactions) are becoming the standard tool for studying features of the halo (as well as the ground state structure of many other unstable and exotic nuclei). Such reactions involve two different mechanisms: diffractive dissociation (in which the projectile is broken up elastically with

the target remaining in its ground state) and stripping (in which the target is excited, often by absorbing the halo neutron). Theoretically, each of these two contributions is evaluated separately. In particular, the stripping cross section can be calculated within a model in which the projectile comprises of the stopped neutron plus the surviving fragment. Such a 'three-body' model (fragment+neutron+target) treats the detected fragment as a 'spectator core' which, at most, interacts elastically with the target. A recent review of knockout reactions can be found in [10].

5 Summary

In this lecture, only a brief introduction to the field of halo nuclei and their theoretical study has been possible. Many topics have not been included and others given only a cursory mention. Luckily, for the practitioner, many recent reviews are now available , describing different aspects of the field from experimental techniques to theoretical models of both structure and reactions. Particular attention was paid here to the interplay between the structure input and the reaction model since this is, on the whole, how the work in this field has developed over the past decade. The lesson has been that in order to obtain a successful description of reactions with halo nuclei, specific features associated with the exotic nature of these systems need to be included, and this has spurred theoretical developments in both structure and reaction studies.

References

1. A.S. Jensen, K. Riisager, D.V. Fedorov and E. Garrido, Rev. Mod. Phys. **76**, 215 (2004).
2. B. Jonson, Phys. Rep., **389**, 1 (2004).
3. J.S. Al-Khalili, F. Nunes, J. Phys. **G 29**, R89 (2003).
4. I. Tanihata, J. Phys. **G 22**, 157 (1996).
5. P.G. Hansen, A.S. Jensen ad B. Jonson, Ann. Rev. Nucl. Part. Sci. **45**, 591 (1995).
6. N. Orr, Nucl. Phys. **A 616**, 155c (1997).
7. R.C. Johnson, *Scattering and reactions of halo nuclei*, The 14th Nishinomiya-Yukawa Memorial Symposium, Nishinomiya, Japan (1999), Prog. Theor. Phys. Supp. **140**, 33 (2000).
8. I.J. Thompson and Y. Suzuki, Nucl. Phys. **A 693**, 424 (2001).
9. R.C. Johnson, *Scattering and reactions of halo nuclei*. Lectures at the VII Hispalensis International Summer School, 11-23 June, 2000, Oramana, Sevilla, Spain, in *An advanced course in modern nuclear physics* (eds. J.M.Arias and M.Lozano, Lecture Notes in Physics series, Springer-Verlag 2001) pp259-291.
10. P.G. Hansen, J.A. Tostevin, Ann. Rev. Nucl. Part. Sci. **53**, 219 (2003)
11. I. Tanihata et al., Phys. Rev. Lett. **55**, 2676 (1985).
12. I. Tanihata et al., Phys. Lett. **B 160**, 380 (1985).

13. P.G. Hansen, B. Jonson, Europhys. News **4**, 409 (1987).
14. T. Bjerge, K.J. Borgström, Nature **138**, 400 (1936).
15. A.M. Poskanzer, S.W. Cosper, Earl K. Hyde and Joseph Cerny, Phys. Rev. Lett. **17**, 1271 (1966).
16. D.J. Millener, J.W. Olness, E.K. Warburton, S. Hanna, Phys. Rev. C **28**, 497 (1983).
17. J.S. Al-Khalili, J.A. Tostevin, Phys. Rev. Lett. **76** 3903 (1996).
18. J.S. Al-Khalili, J.A. Tostevin, I.J. Thompson Phys. Rev. C **54** 1843 (1996).
19. A.S. Jensen, K. Riisager, Phys. Lett. B **470**, 39 (2000).
20. K. Riisager, D.V. Fedorov, A.S. Jensen, Europhys. Lett. **49**, 547 (2000).
21. M.V. Zhukov et al., Phys. Rep. **231**, 151 (1993) .
22. I.J. Thompson and M.V. Zhukov, Phys. Rev. C **53**, 708 (1996).
23. P. Descouvemont, Phys. Rev. C **52**, 704 (1995).
24. K. Varga, Y. Suzuki, Phys. Rev. C **52**, 2885 (1995).
25. Y. Kanada-En'yo, Hisashi Horiuchi, Akira Ono, Phys. Rev. C **52**, 628 (1995).
26. D.V. Fedorov, A.S. Jensen, K. Riisager, Phys. Rev. C **49**, 201 (1994).
27. W. Nazarewicz, M. Ploszajczak, proceedings of this conference.
28. P. Navrátil, W.E. Ormand, Phys. Rev. Lett. **88** 152502 (2002), and references therein.
29. S.C. Pieper and R.B. Wiringa, Annu. Rev. Nucl. Part. Sci. **51**, 53 (2001).
30. D.J. Dean, M. Hjorth-Jensen, Red. Mod. Phys. **75**, 607 (2003).
31. R.J. Glauber, in *Lectures in Theoretical Physics*, ed. W.E. Brittin (Interscience, N.Y., 1959) Vol. 1, 315.
32. P.J. Karol, Phys. Rev. C **11**, 1203 (1974).
33. R. Serber, Phys. Rev. **72**, 1008 (1947).
34. J. Hüfner, M.C. Nemes, Phys. Rev. C **23**, 2538 (1981).
35. E. Sauvan et al., Phys. Lett. B **491**, 1 (2000).
36. M. Kamimura et al., Prog. Theor. Phys. Supp. **89**, 1 (1986).
37. N. Austern et al., Phys. Rep. **154**, 125 (1987).
38. R.C. Johnson, P.J.R. Soper, Phys. Rev. C **1**, 976 (1970).
39. J.S. Al-Khalili, J.A. Tostevin, *Scattering* ed P. Sabatier, E.R. Pike (London Academic) chapter 3.1.3 (2001).
40. J.M. Brooke, J.S. Al-Khalili, J.A. Tostevin, Phys. Rev. C **59**, 1560 (1999).
41. G.D. Alkhazov G D, S.L. Belostotsky, A.A. Vorobyov, Phys. Rep. **42**, 89 (1974).
42. R.C. Johnson, C.J. Goebel, Phys. Rev. C **62**, 027603 (2000).
43. J.A. Tostevin, J.A. Al-Khalili, Phys. Rev. C **59**, R5 (1999).
44. G.R. Satchler, *Direct Nuclear Reactions*, Oxford University Press, 1982.
45. H. Feshbach, *Theoretical Nuclear Physics: Nuclear Reactions*, Wiley, 1993.
46. N.C. Summers, J.S. Al-Khalili and R.C. Johnson, Phys. Rev. C **66** (2002) 014614.
47. R.C. Johnson, J.S. Al-Khalili, J.A. Tostevin, Phys. Rev. Lett. **79**, 2771 (1997).
48. J.D. Harvey, R.C. Johnson, Phys. Rev. C **3**, 636 (1971).
49. A. Bonaccorso, D.M. Brink, Phys. Rev. C **57**, R22 (1998).
50. A. Bonaccorso, D.M. Brink, Phys. Rev. C **58**, 2864 (1998).
51. A. Bonaccorso, Phys. Rev. **60**, 0546041 (1999).
52. V.S. Melezhik and D. Baye, Phys. Rev. C **59**, 3232 (1999).
53. H. Esbensen and G.F. Bertsch, Nucl. Phys. **A 600**, 37 (1996).
54. A. Moro, R. Crespo, F.M. Nunes and I.J. Thompson, Phys. Rev. **C 67**, 047602 (2003).

55. J.S. Al-Khalili *et al.*, Phys. Lett. B **387**, 45 (1996).
56. J.A. Tostevin *et al.*, Phys. Rev. C **56**, R2929 (1997).
57. I.Pecina *et al.*, Phys. Rev. C **52**, 191 (1995).
58. J.J. Kolata *et al.*, Phys. Rev. Lett. **69**, 2631 (1992).
59. M. Lewitowicz *et al.*, Nucl. Phys. **A 562**, 301 (1993).
60. M. Zahar *et al.*, Phys. Rev. C **49**, 1540 (1994).
61. J.S. Al-Khalili, Nucl. Phys. **A 581**, 315 (1995.
62. K. Alder, T. Huus, B. Mottelson and A. Winther, Nucl. Phys. **28**, 432 (1956).